Subcycle dynamics of high-harmonic generation in valence-shell and virtual states of Ar atoms: A self-interaction-free time-dependent density-functional-theory approach

John Heslar, Dmitry A. Telnov, and Shih-I Chu

Phys. Rev. A **91**, 023420 — Published 19 February 2015

DOI: 10.1103/PhysRevA.91.023420

Subcycle dynamics of high-harmonic generation in valence-shell and virtual states of Ar atoms: A self-interaction-free time-dependent-density-functional-theory approach

John Heslar,[1] Dmitry A. Telnov,[2] and Shih-I Chu[1,3,*]

[1] *Center for Quantum Science and Engineering, and Center for Advanced Study in Theoretical Sciences, Department of Physics, National Taiwan University, Taipei 10617, Taiwan*
[2] *Department of Physics, St. Petersburg State University, St. Petersburg 198504, Russia*
[3] *Department of Chemistry, University of Kansas, Lawrence, Kansas 66045, USA*

We perform an *ab initio* all-electron study of the subcycle structure, dynamics, and spectra of high harmonic generation (HHG) processes of Ar atoms in the presence of extreme ultraviolet (XUV) attosecond pulses and near-infrared (NIR) laser fields by means of the *self-interaction-free* time-dependent density functional theory (TDDFT). The TDDFT equations are solved accurately and efficiently via the time-dependent generalized pseudospectral (TDGPS) method. We focus on the subcycle (with respect to NIR field) temporal behavior of the level shift of the excited energy levels and related dynamics of harmonic photon emission. We observe and identify the subcycle shifts in the harmonic emission spectrum as a function of the time delay between the XUV and NIR pulses. In the region where the two pulses overlap, the photon emission peaks have an oscillatory structure with a period of ~ 1.3 fs, which is half of the NIR laser optical cycle. We present and analyze the harmonic emission spectra from $3snp_0$, $3p_0ns$, $3p_1nd_1$, $3p_1np_1$, $3p_0nd_0$, $3p_0np_0$, and $3p_0ns$ excited states and the $3p_04p_0^-$ virtual state as functions of the time delay. In addition, we explore the subcycle a.c. Stark shift phenomenon in NIR fields and its influence on the harmonic emission process. Our analysis reveals several novel features of the subcycle HHG dynamics and spectra as well as temporal energy level shift.

PACS numbers: 32.70.Jz,42.50.Hz,32.80.Qk

I. INTRODUCTION

The study of atomic, molecular, and optical (AMO) processes in ultrashort attosecond (10^{-18} second) laser pulses [1] is one of the most forefront scientific research fields in ultrafast science and technology in the 21st century. In particular, attosecond streaking is among the most exciting latest advances in ultrafast quantum technology [2–8]. Recently, there is a considerable interest in the subcycle a.c. Stark shift and transient absorption spectra [2, 9–13] both theoretically and experimentally. Most observations so far have been made for the He atoms [2, 9, 10] but experimental results on the more complex Ar atoms also now become available [11]. Thus theoretical exploration of the interaction of the Ar atoms with laser fields on the attosecond time scale, including the subcycle photon emission dynamics, is a timely and important subject to study, providing new advancement for the transient harmonic generation dynamics and spectrum.

Regarding the theory of these ultrafast processes, so far most approaches have been based on various single-active-electron (SAE) models [4, 6, 7, 9, 10, 14]. SAE models require only modest computational resources and may appear quite accurate in their predictions. However, they cannot provide a proper treatment of correlated multielectron dynamics which may be crucial for description of ionization and excitation in multielectron targets. Recent experimental studies on attosecond autoionization of argon atoms [11] and attosecond probe spectroscopy of krypton ions [15] clearly show a demand for proper theoretical methods treating ultrafast processes in multielectron quantum systems. The time-dependent density functional theory (TDDFT) can be considered as one of such methods.

Recently, we extended TDDFT for the study of multiphoton single and double ionization of atoms [16], using the time-dependent Krieger-Li-Iafrate exchange-correlation potential with self-interaction correction (TD-KLI-SIC). With the help of the TD-KLI-SIC method, we performed *ab initio* calculations of He, Li and Be atoms in strong near-infared (NIR) laser fields [16, 17] and confirmed that integer discontinuity of the exchange-correlation potential plays an important role in correct description of the ionization processes [17]. Also, with use of our extended TD-KLI-SIC method we uncover for the first time the oscillation structures of the harmonic emission with respect to the time delay between the single attosecond pulse (SAP) and near-infrared (NIR) pulse for He atoms [3]. Using the same TD-KLI-SIC method we helped to identify mechanisms and demonstrate a new regime of phase-matched below-threshold harmonic generation for Ar atoms, for which the generation and phase matching is enabled only near resonance structures of the atomic target [18].

In the present paper, we extend the TD-KLI-SIC approach to *ab initio* exploration of the dynamics of valence-shell electrons in Ar atoms excited by attosecond pulses and driven by near-infrared laser fields. We investigate subcycle (with respect to the NIR field) struc-

* sichu@ku.edu

tures of the photon emission spectra from excited bound states as well as virtual states induced by the laser field. Within the framework of our self-consistent all-electron approach, we study not only the excitations of $3p$ electrons, but also the excitations of more tightly bound $3s$ electrons. We note that unlike the transient absorption, the accompanying process of photon emission has not attracted much attention so far. Of course, radiation of a single atom in this process is weak and somewhat difficult to observe experimentally. However, as in the traditional high-harmonic generation (HHG) process, a measurable efficiency can be reached for the macroscopic signal, when the photon emission from many emitters within an extended medium is in phase [19]. Some experimental techniques can be applied to enhance the yield of high-order harmonics [20]. Recently, we achieved below-threshold phase-matched VUV generation (driven by a linear polarized NIR laser pulse) by field-controlled bound states for Ar atoms in the macroscopic medium [M. Chini *et. al.*, Nat. Photonics 8, 437 (2014)]. In the present study, however, we focus on the detailed all-electron treatment of a single Ar atom, which itself presents a major computational challenge; macroscopic effects related to propagation of the radiation in the medium are beyond the scope of the present paper. Using the TD-KLI-SIC method, we investigate in details the subcycle dynamics of the photon emission (HHG) as a function of the time delay between the attosecond pulse and NIR laser field and provide a benchmark calculation of this process for the Ar atom. In the region where the two pulses overlap, the photon emission peaks have an oscillatory dependence on the time delay with a period of ~ 1.3 fs, which is half of the NIR laser optical cycle. This oscillatory structure is related to the subcycle a.c. Stark shift of the electronic energy levels in the NIR field. We also observe splitting of the emission lines caused by near-resonance multiphoton transition involving NIR and XUV photons, identify its mechanism and explore the role of field-induced virtual states.

The paper is organized as follows. In Sec. II, we extend the TD-KLI-SIC method to study the shifts of the energy levels in the argon atoms on the sub-femtosecond time scale in a two-color two-photon (XUV+NIR) absorption process. To study the sub-laser-cycle dynamics, we probe the excited states of Ar by a single attosecond pulse (SAP) in the XUV frequency range, with the pulse duration near 20 times smaller than the NIR laser period. Section III presents the photon emission energy spectra related to various excited states of Ar and study the effect of the time-delay between the NIR and SAP fields on these spectra. Conclusions and remarks are presented in Sec. IV.

II. THEORETICAL METHOD

TD-KLI-SIC procedure for nonperturbative treatment of atoms in two-color laser fields

The single-particle potential is constructed with the help of the TD-KLI-SIC procedure. The TD-KLI-SIC single-particle potential can be expressed as follows:

$$V^{\rm s}_\sigma(\boldsymbol{r},t) = \sum_{i=1}^{N_\sigma} \frac{\rho_{i\sigma}(\boldsymbol{r},t)}{\rho_\sigma(\boldsymbol{r},t)} \left[v_{i\sigma}(\boldsymbol{r},t) + \bar{V}^{\rm s}_{i\sigma} - \bar{v}_{i\sigma} \right]. \quad (1)$$

Here indices i and σ enumerate spin-orbitals (σ corresponds to the spin projection, N_σ is the total number of electrons with the spin σ). The spin-orbital densities $\rho_{i\sigma}$ and total spin-densities ρ_σ are given by

$$\begin{aligned} \rho_{i\sigma}(\boldsymbol{r},t) &= |\psi_{i\sigma}(\boldsymbol{r},t)|^2, \\ \rho_\sigma(\boldsymbol{r},t) &= \sum_{i=1}^{N_\sigma} \rho_{i\sigma}(\boldsymbol{r},t), \end{aligned} \quad (2)$$

($\psi_{i\sigma}(\boldsymbol{r},t)$ is the Kohn-Sham spin-orbital). The orbital-dependent potential $v_{i\sigma}(\boldsymbol{r},t)$ includes the Hartree and exchange-correlation parts as well as self-interaction corrections. The mean values $\bar{V}^{\rm s}_{i\sigma}$ and $\bar{v}_{i\sigma}$ are calculated with the spin-densities $\rho_{i\sigma}(\boldsymbol{r},t)$:

$$\begin{aligned} \bar{V}^{\rm s}_{i\sigma} &= \int d^3r \rho_{i\sigma}(\boldsymbol{r},t) V^{\rm s}_\sigma(\boldsymbol{r},t), \\ \bar{v}_{i\sigma} &= \int d^3r \rho_{i\sigma}(\boldsymbol{r},t) v_{i\sigma}(\boldsymbol{r},t). \end{aligned} \quad (3)$$

A more detailed description of our TD-KLI-SIC procedure can be found elsewhere [16, 21, 22].

To obtain the time-dependent electron densities and calculate the induced dipole moments, one has to solve a set of the time-dependent Kohn-Sham equations [23] for the spin-orbitals $\psi_{i\sigma}(\boldsymbol{r},t)$:

$$\begin{aligned} i\frac{\partial}{\partial t}\psi_{i\sigma}(\boldsymbol{r},t) = \Big[&-\frac{1}{2}\nabla^2 - \frac{Z}{r} + V^{\rm s}_\sigma(\boldsymbol{r},t) \\ &+ v_{\rm ext}(\boldsymbol{r},t) \Big] \psi_{i\sigma}(\boldsymbol{r},t), \quad i = 1, ..., N_\sigma. \end{aligned} \quad (4)$$

Here $Z = 18$ is the nucleus charge; $v_{\rm ext}$ is the interaction of the electron with the external fields. We assume that the external fields are polarized along the z direction:

$$v_{\rm ext}(\boldsymbol{r},t) = -z[E_{\rm X}(t) + E_{\rm L}(t)]. \quad (5)$$

The SAP field can be expressed as follows:

$$E_{\rm X}(t) = F_{\rm X} \exp\left(-\frac{2\ln 2 t^2}{\tau^2_{\rm X}} \right) \cos(\omega_{\rm X} t). \quad (6)$$

Here, $F_{\rm X}$ is the peak field strength of the SAP, $\tau_{\rm X} = 140$ as is its full width at half maximum (FWHM), and $\omega_{\rm X} = 15$ eV is its central frequency. The SAP peak

intensity is 1×10^{10} W/cm^2. The NIR laser field has the form:

$$E_{\rm L}(t) = F_{\rm L} \exp\left(-\frac{2\ln 2(t-t_d)^2}{\tau_{\rm L}^2}\right) \cos[\omega_{\rm L}(t-t_d)]. \quad (7)$$

Here, $F_{\rm L}$ is the peak field strength of the NIR laser pulse, $\tau_{\rm L} = 6$ fs is its FWHM, and $\omega_{\rm L}$ is the central frequency of the NIR field (here we choose the laser wavelength as 750 nm [$\omega_{\rm L} = 1.65$ eV]). The NIR laser peak intensity is 1×10^{13} W/cm^2. The parameter t_d denotes the time delay between the NIR pulse and the SAP; the negative (positive) time delay refers to the NIR pulse (SAP) arriving first.

After the time-dependent spin-orbitals $\psi_{i\sigma}$ are obtained, the induced dipole moment and dipole acceleration can be expressed as follows:

$$\boldsymbol{d}(t) = \sum_{i\sigma} \langle \psi_{i\sigma}(\boldsymbol{r},t)|\boldsymbol{r}|\psi_{i\sigma}(\boldsymbol{r},t)\rangle, \quad (8)$$

$$\boldsymbol{a}(t) = \sum_{i\sigma} \langle \psi_{i\sigma}(\boldsymbol{r},t)|\nabla\left[\frac{Z}{r} - v_{\rm ext}(\boldsymbol{r},t)\right]|\psi_{i\sigma}(\boldsymbol{r},t)\rangle. \quad (9)$$

The dipole moment and dipole acceleration satisfy the same relation as the corresponding classical quantities:

$$\frac{d^2}{dt^2}\boldsymbol{d}(t) = \boldsymbol{a}(t). \quad (10)$$

The expression for $\boldsymbol{a}(t)$ can be derived from that for $\boldsymbol{d}(t)$ with the help of the Ehrenfest theorem. We note that only the nuclear and external field potentials are present in Eq. (9) since the *exact* exchange-correlation potential *does not* contribute to the expectation value of acceleration [24]. The spectral density of the radiation energy is given by the following expression:

$$S(\omega) = \frac{2}{3\pi c^3}\left|\int_{-\infty}^{\infty} \boldsymbol{a}(t)\exp(-i\omega t)dt\right|^2. \quad (11)$$

Here ω is the frequency of radiation, c is the velocity of light. $S(\omega)$ has the meaning of the energy emitted per unit frequency range at the particular photon frequency ω.

To solve the set of equations (4), we apply the time-dependent generalized pseudospectral (TDGPS) method [25] which proved accurate and efficient treatment in our previous TDDFT calculations (see, *e. g.*, Refs. [16, 21, 26, 27]). For the TDGPS discretization in the present calculations, we use 256 radial and 32 angular grid points, and the time step 0.02 a.u. Eq. (4) is solved in space within a sphere with the radius 100 a.u.; between 70 a.u. and 100 a.u. we place an absorber. Absorbed parts of the wave packet localized beyond 70 a.u. describe unbound states populated during the ionization process. The time delay was varied in steps of $\Delta t_d = 100$ as within the range of -14 fs $\leq t_d \leq 14$ fs (280 steps in total), with $t_d = 0$ corresponding to both SAP and NIR pulse envelopes centered at $t = 0$.

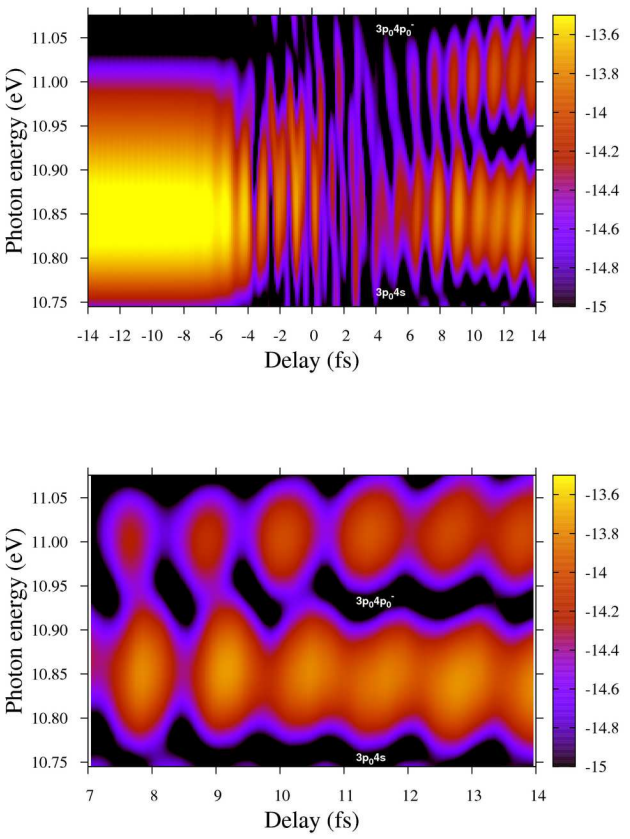

FIG. 1. (Color online) Photon emission energy spectrum of the $3p_04s$ excited state and the $3p_04p_0^-$ virtual state as a function of the time delay between the NIR pulse and SAP. The yellow color indicates the highest energy emitted. The color bars are represented by the $\log_{10} S(\omega)$ of the spectral density in Eq. (11). Negative delays indicate the NIR pulse arrives on target before the SAP. One-NIR laser optical cycle is equal to 2.5 fs.

III. RESULTS AND DISCUSSIONS

The ground state of argon can be described by the electron configuration $1s^22s^22p^63s^23p^6$. In the present paper, our main focus is on the response of the individual valence-shell electrons ($3s$ and $3p$) to the NIR and XUV laser fields. All eighteen electrons are treated explicitly in the calculation and we found the inner-shell electrons do not participate appreciably in the multi-photon processes. Here, we discuss only the valence-shell electrons. The TD-KLI-SIC and experimental values for the binding energy of the $3p$ electron are, respectively, 0.550 and 0.580 a.u., while the corresponding values for the $3s$ electron are 1.050 and 1.077 a.u. When an argon atom absorbs a photon from the XUV field with the intensity 1×10^{10} W/cm^2, it can be excited with a substantial probability from the ground state to one of many singly excited states or to the continuum, depending on the

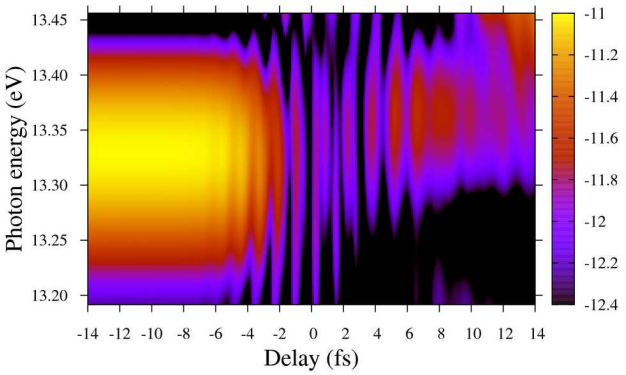

FIG. 2. (Color online) Photon emission energy spectrum of the $3p_0 3d_0$ excited state as a function of the time delay between the NIR pulse and SAP. The yellow color indicates the highest energy emitted. The color bars are represented by the $\log_{10} S(\omega)$ of the spectral density in Eq. (11). Negative delays indicate the NIR pulse arrives on target before the SAP.

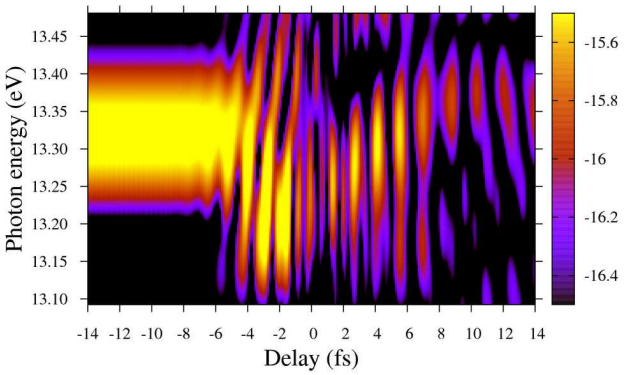

FIG. 3. (Color online) Photon emission energy spectrum of the $3p_1 3d_1$ excited state as a function of the time delay between the NIR pulse and SAP. The yellow color indicates the highest energy emitted. The color bars are represented by the $\log_{10} S(\omega)$ of the spectral density in Eq. (11). Negative delays indicate the NIR pulse arrives on target before the SAP.

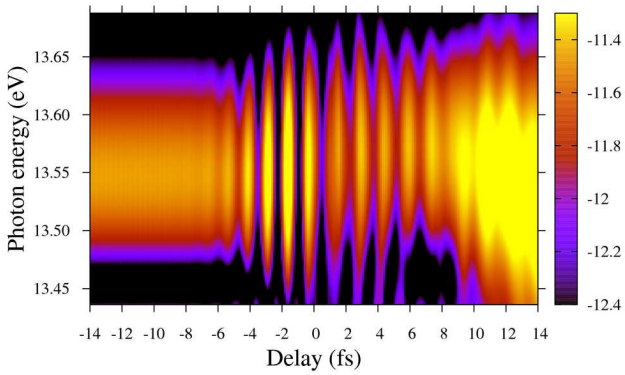

FIG. 4. (Color online) Photon emission energy spectrum of the $3p_0 5s$ excited state as a function of the time delay between the NIR pulse and SAP. The yellow color indicates the highest energy emitted. The color bars are represented by the $\log_{10} S(\omega)$ of the spectral density in Eq. (11). Negative delays indicate the NIR pulse arrives on target before the SAP.

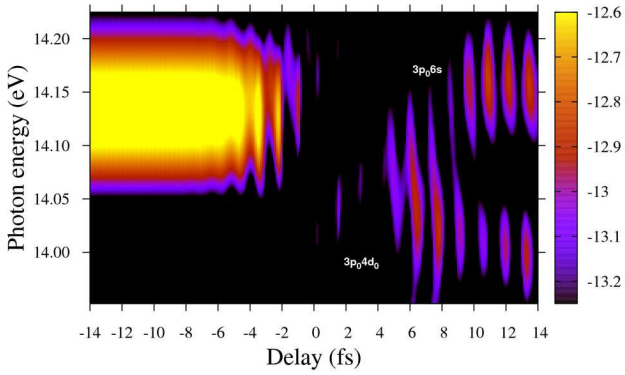

FIG. 5. (Color online) Photon emission energy spectrum of the $3p_0 6s$ or $3p_0 4d_0$ (near resonance) excited states as a function of the time delay between the NIR pulse and SAP. The yellow color indicates the highest energy emitted. The color bars are represented by the $\log_{10} S(\omega)$ of the spectral density in Eq. (11). Negative delays indicate the NIR pulse arrives on target before the SAP.

energy of the XUV photon absorbed. Possible singly excited states are $3snp_0$, $3p_1nd_1$, $3p_0ns$ or $3p_0nd_0$. In this notation, the first two symbols indicate the initial subshell of the excited electron ($3s$, $3p_0$ or $3p_1$); the last two symbols show the destination of the electron after transition (np_0, nd_0, ns or nd_1). The subscript describes the angular momentum projection onto the field direction, which is polarized along the z axis. Thus $3p_1$ denotes the $3p$ electron with the angular momentum projection on the z axis equal to 1. Due to the cylindrical symmetry, the response of the $3p_1$ and $3p_{-1}$ orbitals to the linear polarized laser fields is identical. Thus, in the following, all the $3p_1$ results refer to the total contributions due to two electrons in the $3p_1$ and two electrons in the $3p_{-1}$ subshells (total of four electrons).

For the valence-shell electrons, the ionization probability is mainly affected by the binding energy of the orbital: the smaller the binding energy, the larger the ionization probability. For Ar, the binding energy of the $3p$ orbital is about 0.5 a.u. smaller than that of the $3s$ orbital. Among the $3p$ electrons, the ionization probability is further affected by the geometrical factor: for the $3p_1$ orbital, where the laser field polarization is parallel to the

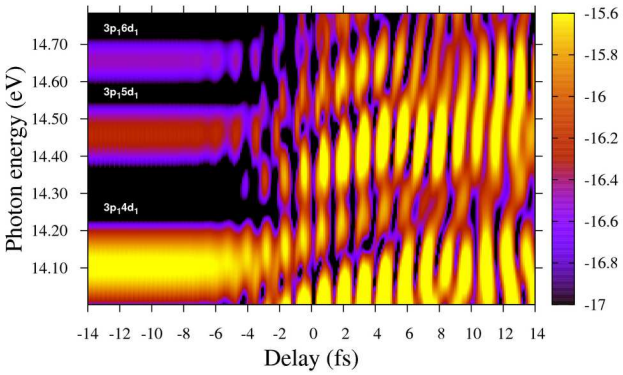

FIG. 6. (Color online) Photon emission energy spectrum of the $3p_1nd_1$ (n =4,5, and 6) excited states as a function of the time delay between the NIR pulse and SAP. The yellow color indicates the highest energy emitted. The color bars are represented by the $\log_{10} S(\omega)$ of the spectral density in Eq. (11). Negative delays indicate the NIR pulse arrives on target before the SAP.

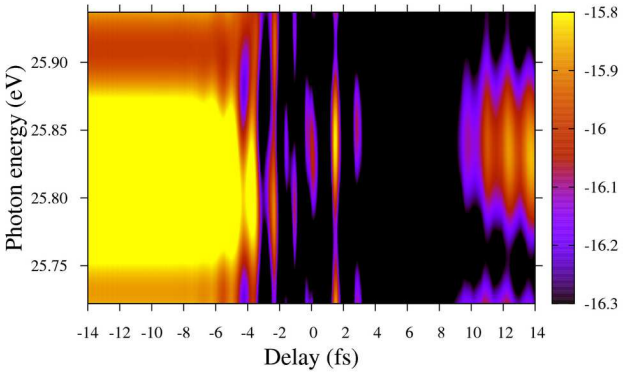

FIG. 7. (Color online) Photon emission energy spectrum of the $3s4p_0$ excited state as a function of the time delay between the NIR pulse and SAP. The yellow color indicates the highest energy emitted. The color bars are represented by the $\log_{10} S(\omega)$ of the spectral density in Eq. (11). Negative delays indicate the NIR pulse arrives on target before the SAP.

node line, the ionization probability is generally smaller than that for the $3p_0$ orbital, where the field direction is perpendicular to the nodal plane. Therefore, we can expect that the $3p_0$ electrons will be most easily ionized, followed by the $3p_1$ electrons and then the $3s$ electrons. This general order can be changed by the multiphoton resonance effect that can lead to the enhancement of the ionization of the particular orbital.

In contrast with the XUV field, the NIR laser intensity (1×10^{13} W/cm^2) used is weak for the excitation of the ground state, that is why we do not see any effects in the photon emission spectrum (Figs. 1-7) when the NIR pulse comes first (-14 fs $\leq t_d \leq -5$ fs). However, the NIR field is strong for the excited states, so when the NIR pulse comes after the SAP (positive t_d), further one-photon transitions $3snp_0 \rightarrow 3sn'd_0$, $3snp_0 \rightarrow 3sn's$, $3p_0nd_0 \rightarrow 3p_0n'p_0$, $3p_0nd_0 \rightarrow 3p_0n'f_0$, $3p_0ns \rightarrow 3p_0n'p_0$, $3p_1nd_1 \rightarrow 3p_1n'p_1$, and $3p_1nd_1 \rightarrow 3p_1n'f_1$ can occur, or the atom can be ionized. Here, we deal with a broad, continuous spectrum of the SAP ($\sim$ 15 eV to the first ionization potential of Ar) which allows us to observe subsequent photon emission from each populated individual excited state simultaneously.

Some of the higher excited states are shifted by the ponderomotive potential U_p of the NIR field, where $U_p = F_L^2/(2\omega_L)^2$; for the field strength and frequency used, $U_p = 0.53$ eV. Here, the time delay is in the range -14 fs $\leq t_d \leq 14$ fs. Next, we will discuss the photon emission from each of the excited states individually as a function of the time delay t_d.

The density plots of the photon emission spectra in Figs. (1-7) depict the transitions from $3p_04s$ ($\sim$ 10.85 eV), $3p_04p_0^-$ ($\sim$ 11 eV) [$3p_04p_0^-$ is a laser-induced virtual state; the symbols $3p_04p_0$ refer to the real excited state, and the superscript minus indicates that one NIR photon is emitted, so the energy of $3p_04p_0^-$ is less by ω_L than the energy of $3p_04p_0$], $3p_m3d_m$ ($m = 0$ or 1; $\sim$ 13.32 eV), $3p_05s$ ($\sim$ 13.55 eV), $3p_06s$ or $3p_m4d_m$ (near resonance; $\sim$ 14.15 eV), $3p_15d_1$ ($\sim$ 14.45 eV), $3p_16d_1$ ($\sim$ 14.65 eV), and $3s4p_0$ ($\sim$ 25.85 eV) as functions of t$_d$. For the NIR and XUV pulses polarized along the z direction, the projection of the electron angular momentum on the z axis is conserved. Hence, nl_m states can have transitions to other $n'l'_{m'}$ excited states, only when the magnetic quantum numbers are equal ($m = m'$). Plotting the photon emission spectra as functions of the time delay results in a broadened and shifted (streaked) spectra (Figs. 1-7). Also, in the region where the NIR pulse and SAP overlap (-4 fs $\leq t_d \leq 4$ fs), the photon emission lines have oscillations with a period of $\sim$ 1.3 fs, which is half of the NIR laser optical cycle, and this is a manifestation of the instantaneous shift of the electronic energy levels in the NIR laser field (more precisely, one should talk about the laser-induced phase related to the instantaneous Stark shift [12, 13, 29]). This phenomenon was also observed in recent experimental works [2, 9] where the transient absorption technique was used.

In Fig. 1 we observe splitting of the lines in the photon emission spectrum into sub-lines near $t_d \sim$5 fs. The additional (virtual state) line has been identified as contribution from the excitation of the dressed $3p_04p_0$ state, after emitting one NIR photon ($3p_04p_0^-$). The line splitting here has the same nature as in the He atom [2, 3] and can be explained by emission from the virtual states which emerge when the atomic levels are dressed by the NIR field. It can be also described in terms of two-photon absorption and emission processes. First, absorption of one XUV photon excites the ground state to the $3p_04s$ state. The latter is strongly coupled to the $3p_04p_0$ state

by the NIR field because these two states are in the vicinity of a one-photon resonance. Thus absorption of one XUV photon and one NIR photon populates the $3p_04p_0$ state. Then a reverse process of photon emission takes place. Emission of a single NIR photon leads to the transition to the virtual $3p_04p_0^-$ state. Since the resonance conditions are not exactly satisfied, the energies of the $3p_04s$ and $3p_04p_0^-$ states are slightly different, subsequent transition to the ground state results in emission of the XUV photons with slightly different frequencies, that is line splitting.

Since in our TD-KLI-SIC approach all electrons are treated on the same footing, the photon emission spectra contain not only the lines caused by excitations of the $3p$ electrons but also the lines resulting from excitations of the $3s$ subshell, which has a larger ionization potential. In Fig. 7, we show the photon emission spectrum from the $3s4p_0$ excited state, where the photon energies are above the first ionization threshold of Ar. As one can see, in the region where the NIR field and SAP overlap, the photon emission line exhibits similar oscillations with the period equal to one half of the NIR optical cycle.

IV. CONCLUSION

In summary, we have performed a *ab initio* and comprehensive investigation of the subcycle dynamical behavior of HHG (photon emission) by Ar atoms at different time delays between the SAP and NIR pulses, using the *self-interaction-free* TDDFT approach and the accurate TDGPS time propagation method. We employ the TD-KLI-SIC method for construction of the exchange-correlation potential with the proper long-range dependence on the coordinate, which allows accurate description of the ground and singly excited states in Ar. We have explored the subcycle dynamical behavior of the emission lines corresponding to the transitions from the $3p_04s$, $3p_m3d_m$ ($m = 0$ or 1), $3p_05s$, $3p_06s$, $3p_m4d_m$, $3p_15d_1$, $3p_16d_1$, and $3snp_0$ excited states and the $3p_04p_0^-$ virtual state on a sub-femtosecond time scale as a function of the time delay between the SAP and NIR fields. We observe that the photon emission spectra oscillate as a function of the time delay with a period equal to one half of the NIR laser optical cycle. In addition, we find the near-resonance multiphoton transition from the ground state involving NIR and XUV photons causes splitting in the emission lines of the $3p_04s$ and $3p_06s$ excited states. We have identified the mechanisms responsible for the observed subcycle HHG line splitting and dynamical Stark shift. Also, when the NIR and SAP laser fields are overlapped in time, new features in the photon emission spectra appear, corresponding to the virtual intermediate states in the two-photon excitation to bound states which cannot be populated by a single pulse alone. To our knowledge, no other theoretical work on oscillation structures of the harmonic emission with respect to the time delay between the SAP and NIR pulse for Ar atoms exist at this moment in time.

ACKNOWLEDGMENTS

This work was partially supported by the Chemical Sciences, Geosciences and Biosciences Division of the Office of Basic Energy Sciences, Office of Sciences, U. S. Department of Energy. We also acknowledge the partial support of the Ministry of Science and Technology of Taiwan and National Taiwan University (Grants No. 103R104021 and No. 103R8700-2). D.A.T. acknowledges the partial support of St. Petersburg State University (Grant No. 11.38.654.2013).

[1] F. Krausz, and M. Ivanov, Rev. Mod. Phys. **81**, 163 (2009).
[2] M. Chini, X. Wang, Y. Cheng, Y. Wu, D. Zhao, D. A. Telnov, S. I. Chu, and Z. Chang, Sci. Rep. **3**, 1105 (2013).
[3] J. Heslar, D. A. Telnov, and S. I. Chu, Phys. Rev. A **89**, 052517 (2014).
[4] M. Schultze, M. Fieß , N. Karpowicz, J. Gagnon, M. Korbman, M. Hofstetter, S. Neppl, A. L. Cavalieri, Y. Komninos, Th. Mercouris, C. A. Nicolaides, R. Pazourek, S. Nagele, J. Feist, J. Burgdörfer, A. M. Azzeer, R. Ernstorfer, R. Kienberger, U. Kleineberg, E. Goulielmakis, F. Krausz, and V. S. Yakovlev, Science **328**, 1658 (2010).
[5] G. Sansone, E. Benedetti, F. Calegari, C. Vozzi, L. Avaldi, R. Flammini, L. Poletto, P. Villoresi, C. Altucci, R. Velotta, S. Stagira, S. De Silvestri, and M. Nisoli, Science **314**, 443 (2006).
[6] X. M. Tong, P. Ranitovic, C. L. Cocke, and N. Toshima, Phys. Rev. A **81**, 021404(R) (2010).
[7] X. M. Tong and N. Toshima, Phys. Rev. A **81**, 063403 (2010).
[8] R. Pazourek, J. Feist, S. Nagele, and J. Burgdörfer, Phys. Rev. Lett. **108**, 163001 (2012).
[9] M. Chini, B. Zhao, H. Wang, Y. Cheng, S. X. Hu, and Z. Chang, Phys. Rev. Lett. **109**, 073601 (2012).
[10] S. Gilbertson, M. Chini, X. Feng, S. Khan, Y. Wu, and Z. Chang, Phys. Rev. Lett. **105**, 263003 (2010).
[11] H. Wang, M. Chini, S. Chen, C. H. Zhang, F. He, Y. Cheng, Y. Wu, U. Thumm, and Z. Chang, Phys. Rev. Lett. **105**, 143002 (2010).
[12] S. Chen, M. Wu, M. B. Gaarde, and K. J. Schafer, Phys. Rev. A **87**, 033408 (2013).
[13] S. Chen, M. Wu, M. B. Gaarde, and K. J. Schafer, Phys. Rev. A **88**, 033409 (2013).
[14] S. Chen, M. J. Bell, A. R. Beck, H. Mashiko, M. Wu, A. N. Pfeiffer, M. B. Gaarde, D. M. Neumark, S. R. Leone, and K. J. Schafer, Phys. Rev. A **86**, 063408 (2012).
[15] E. Goulielmakis, Z.-H. Loh, A. Wirth, R. Santra, N. Rohringer, V. S. Yakovlev, S. Zherebtsov, T. Pfeifer, A. M. Azzeer, M. F. Kling, S. R. Leone, and F. Krausz,

Nature **466**, 739 (2010).
[16] D. A. Telnov, J. Heslar, and S. I. Chu, Chem. Phys. **391**, 88 (2011).
[17] J. Heslar, D. A. Telnov, and S. I. Chu, Phys. Rev. A **87**, 052513 (2013).
[18] M. Chini, X. Wang, Y. Cheng, H. Wang, Y. Wu, E. Cunningham, P. -C. Li, J. Heslar, D. A. Telnov, S. I. Chu, and Z. Chang, Nat. Photonics **8**, 437 (2014).
[19] M. J. J. Vrakking, Phys. Chem. Chem. Phys. **16**, 2775 (2014).
[20] X. Wang, M. Chini, Q. Zhang, K. Zhao, Y. Wu, D. A. Telnov, S. I. Chu, and Z. Chang, Phys. Rev. A **86**, 021802(R) (2012).
[21] X. M. Tong and S. I. Chu, Phys. Rev. A **57**, 452 (1998).
[22] X. M. Tong and S. I. Chu, Phys. Rev. A **55**, 3406 (1997).
[23] W. Kohn and L. J. Sham, Phys. Rev. **140**, A1113 (1965).
[24] G. Vignale, Phys. Rev. Lett. **74**, 3233 (1995).
[25] X. M. Tong and S. I. Chu, Chem. Phys. **217**, 119 (1997).
[26] J. J. Carrera and S. I. Chu, Phys. Rev. A **79**, 063410 (2009).
[27] S. I. Chu and D. A. Telnov, in *Computational Studies of New Materials II: From Ultrafast Processes and Nanostructures to Optoelectronics, Energy Storage and Nanomedicine*, edited by T. F. George, D. Jelski, R. R. Letfullin, and G. Zhang (World Scientific, New Jersey, 2011), pp. 75–101.
[28] X. M. Tong and S. I. Chu, Phys. Rev. A **64**, 013417 (2001).
[29] A. Wirth, M. Th. Hassan, I. Grguraš, J. Gagnon, A. Moulet, T. T. Luu, S. Pabst, R. Santra, Z. A. Alahmed, A. M. Azzeer, V. S. Yakovlev, V. Pervak, F. Krausz, and E. Goulielmakis, Science **334**, 195 (2011).